Cross sections and analyzing powers for $(\vec{p},np)$ reactions of ^{2}H, ^{6}Li, and ^{12}C at 296 MeV

T. Wakasa,[1,*] J. Yasuda,[1] M. Dozono,[2] T. Fukunaga,[1] S. Gotanda,[3] K. Hatanaka,[4] K. Ishibashi,[1] Y. Kanaya,[3] S. Kimura,[1] Y. Maeda,[3] Y. Maeda,[1] Y. Nishio,[1] T. Noro,[1] T. Nozoe,[1] K. Ohnaka,[1] S. Sakaguchi,[1] Y. Sakemi,[2] K. Sekiguchi,[5] T. Taguchi,[5] and Y. Wada[5]

[1]*Department of Physics, Kyushu University, Nishi, Fukuoka 819-0395, Japan*
[2]*Center for Nuclear Study, University of Tokyo, Bunkyo, Tokyo 113-0033, Japan*
[3]*Department of Applied Physics, University of Miyazaki, Miyazaki, Miyazaki 889-2192, Japan*
[4]*Research Center for Nuclear Physics, Osaka University, Ibaraki, Osaka 567-0047, Japan*
[5]*Department of Physics, Tohoku University, Sendai, Miyagi 980-8578, Japan*

(Received 17 December 2016; revised manuscript received 8 April 2017; published 10 July 2017)

We report measurements of cross sections and analyzing powers for nucleon-knockout $(\vec{p},np)$ reactions of ^{2}H, ^{6}Li, and ^{12}C at 296 MeV using the RCNP NPOL3 neutron detector and large acceptance spectrometer. The $1s$ and $1p$ knockout reactions were successfully separated with a separation-energy resolution of approximately 6 MeV. The resulting data were compared with plane-wave and distorted-wave impulse approximation calculations employing the nucleon-nucleon t matrix in free space. No significant differences were identified in the case of the present analyzing power data, in contrast to the significant reductions observed in $(\vec{p},2p)$ values. The conventional Pauli blocking and nuclear binding effects with the g matrix and the relativistic effect of nucleon mass reduction in the nuclei are also discussed.

DOI: 10.1103/PhysRevC.96.014604

I. INTRODUCTION

The data acquired from (p,p') and (p,n) reactions provide a means of studying the effects of the nuclear mean field on nucleon-nucleon (NN) interactions through polarization observables [1,2]. At present, modifications of NN interactions in a nuclear medium through Pauli blocking and nuclear binding effects are typically investigated using the relativistic Dirac-Brueckner-Hartree-Fock (DBHF) theory [3–6]. The DBHF approach is known to account for the three-nucleon force effects that are crucial to nuclear saturation [7]. However, polarization observables for quasielastic scattering [8] and the excitation of unnatural-parity states [9–12] cannot be explained based on these conventional medium effects. As an example, the data for the stretched 6^{-}, $T = 1$ state in ^{28}Si show a larger spin-orbit contribution to the tensor interactions as well as some changes in the tensor interactions [12]. For this reason, the nonconventional effects resulting from the reductions of both the hadron mass and the coupling constant with increasing nuclear density have been discussed as a signature of the partial restoration of chiral symmetry in nuclear matter [13–15]. Sammarruca *et al.* [16] investigated the effects of density-dependent meson mass reductions on these data, and concluded that these effects are essentially absent, because the average densities are low for the stretched transitions. It should be noted that, in the case of nucleon knockout $(p,2p)$ and (p,np) reactions, a significant contribution can be expected from high-density nuclear interiors [17].

The analyzing power, A_y, for the $(p,2p)$ reaction shows a reduction compared with the relevant value for proton-proton scattering. The reduction of A_y was first observed at TRIUMF for the $1s$ knockout $(p,2p)$ reaction of ^{16}O at a proton incident energy of $T_0 = 500$ MeV [18]. The extended studies involving many target nuclei at $T_0 = 392$ MeV performed at RCNP subsequently demonstrated that the A_y values are systematically reduced as a function of either the separation energy or effective mean density [19]. This reduction in analyzing power can be explained theoretically, at least in part, as a result of the lower nucleon mass in the strong scalar part of the relativistic nuclear potential [20]. Other factors leading to the reduction can be determined by considering modifications of the meson mass and coupling constant in nuclei [21]. It is necessary to point out, however, that there are significant uncertainties and correlations in these modified values, since the A_y data alone do not exclusively determine the NN interaction.

In contrast to the $(p,2p)$ reaction, the A_y data for the (p,np) reaction at $T_0 = 200$ MeV [22] and 392 MeV [23,24] show no significant reduction relative to the values obtained from proton-neutron scattering. This difference between the $(p,2p)$ and (p,np) reactions suggests that the medium effects of the NN interaction vary with the isospin. Thus, further systematic investigations of the (p,np) reaction are required to assess the isospin dependence of these effects.

In this paper, we present the cross sections and analyzing powers for neutron knockout (p,np) reactions of ^{2}H, ^{6}Li, and ^{12}C at $T_0 = 296$ MeV. The nucleon knockout reaction mechanism is expected to be relatively simple within this range of incident energies [20,25], thereby enabling us to assess the nuclear medium effects on the NN interaction. Herein, the data from these reactions are compared with the results of plane-wave and distorted-wave impulse approximation (PWIA and DWIA) calculations employing the NN t matrix in free space. No significant differences were observed between our (p,np) data and the theoretical results, thereby demonstrating

*wakasa@phys.kyushu-u.ac.jp; http://ne.phys.kyushu-u.ac.jp/~wakasa

the isospin dependence of the medium effects of the NN interaction.

II. EXPERIMENTAL METHODS

Measurements were performed using the West-South Beam Line (WS-BL) [26] at the Research Center for Nuclear Physics (RCNP), Osaka University. The beam line configuration and the doubly achromatic beam properties have been reported previously [26]. Therefore, the following text discusses solely the experimental details unique to the present experimentation.

A. Polarized proton beam

A polarized proton beam generated by a high-intensity polarized ion source (HIPIS) [27] was accelerated to $T_0 = 53$ and 296 MeV using an azimuthally varying field (AVF) [28] and ring [29] cyclotrons, respectively. The beam polarization direction was reversed every 5 s by selecting rf transitions so as to minimize false geometric asymmetries. During the (p,n) experiments, one out of nine beam pulses was selected for injection into the ring cyclotron, resulting in a beam pulse period of 584 ns. This pulse selection reduced the wraparound of slow neutrons from preceding beam pulses. In contrast, pulse selection was not performed throughout the (p,np) measurements in order to obtain reasonable statistical accuracy. The beam pulse period was kept constant by implementing single-turn extraction from the ring cyclotron during the measurements. Multiturn extracted protons were found to account for less than 1% of the single-turn extracted protons.

The beam polarization was continuously monitored using the BLP1 beam-line polarimeter [26]. This device consisted of four pairs of conjugate-angle plastic scintillators, and determined the beam polarization via $^1\mathrm{H}(\vec{p},p)^1\mathrm{H}$ scattering. A self-supporting polyethylene (CH_2) target with a thickness of 1.1 mg/cm^2 was used as the hydrogen target, and both elastically scattered and recoiled protons were detected with kinematical coincidence using a pair of scintillators. The beam polarization magnitude had a typical value of approximately 0.40. The systematic uncertainty of the analyzing power data was estimated to be approximately 2% based on the uncertainty of the beam polarization [30].

B. Targets and dipole magnet

The proton beam bombarded self-supporting CD_2 (deuterated polyethylene), enriched ^{6}Li ($\geqslant$99% ^{6}Li), and natural C (98.9% ^{12}C) targets with thicknesses of 16.7, 15.4, and 16.8 mg/cm^2, respectively. Protons downstream of the targets were transported to a graphite beam dump (a Faraday cup), at which point the beam current was measured. Typical beam currents used for the (p,n) and (p,np) measurements were 25 and 130 nA, respectively.

A dipole magnet made of permanent NEOMAX magnets [31] was installed 10 cm downstream from the target. This magnet had a magnetic rigidity of $B\rho = 0.95$ Tm, which was sufficient to sweep charged particles from the target in order to prevent them from entering the neutron detector system.

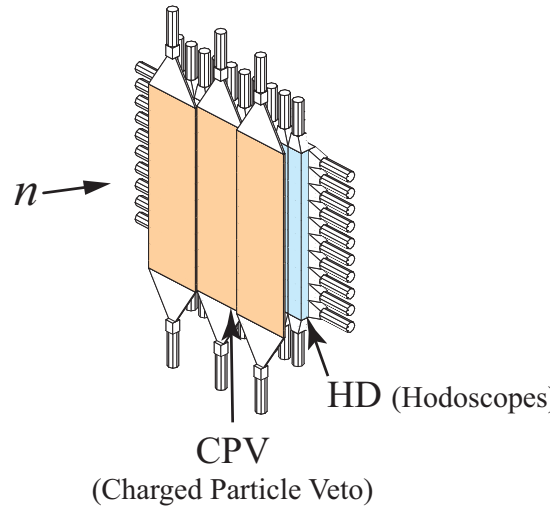

FIG. 1. Schematic view of the NPOL3 neutron detector system.

C. Neutron and proton measurements

The two outgoing nucleons (a neutron and a proton) from the target were measured simultaneously using the NPOL3 neutron detector system [32] and the Large Acceptance Spectrometer (LAS) [33].

Neutrons were detected with a 20 m flight path length at $\theta_n = 22^\circ$. As shown in Fig. 1, the neutron detector system (HD1 and HD2) consisted of 20 sets of one-dimensional position-sensitive plastic scintillators (BC408) with a size of $100 \times 10 \times 5\,\mathrm{cm}^3$. Thin plastic scintillation detectors (CPV) placed in front of HD1 were used to distinguish charged particles from neutrons.

The momenta of protons were determined by the LAS at $\theta_p = 65^\circ$. The LAS consisted of quadrupole and dipole magnets and was designed to realize a large solid angle ($\simeq$20 msr) and a wide momentum acceptance range ($\pm$15%). The angle setting and the central energy of the LAS corresponded to the kinematic conditions for free $p + n$ scattering. The solid angle was restricted to 9.0 msr using a copper collimator positioned at the entrance to the LAS, and the horizontal and vertical angle widths were $\pm$50 and $\pm$45 msr, respectively. At the focal plane of the LAS, a one-dimensional position-sensitive plastic scintillator with a size of $200 \times 15 \times 0.6\,\mathrm{cm}^3$ was used, such that the positions of the detected protons could be reconstructed. The energy resolution was determined by measuring the $p + p$ elastic scattering obtained with a CH_2 target with a thickness of 16.8 mg/cm^2. Using this method, the resolution was found to be 4 MeV with regard to the full width at half maximum (FWHM).

III. DATA REDUCTION

A. Neutron detection efficiency and energy resolution

The neutron detection efficiency was determined using the quasielastic $^{12}\mathrm{C}(p,n)$ reaction at $\theta_{\mathrm{lab}} = 22^\circ$, for which the cross section at $T_0 = 296$ MeV is known [34]. The resulting efficiency was 0.073 ± 0.004, with the overall uncertainty primarily arising from uncertainties in the cross section and

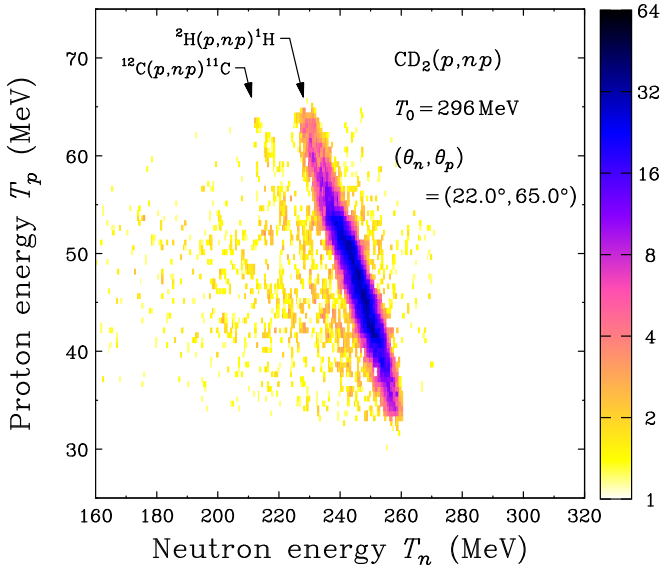

FIG. 2. Neutron kinetic energy T_n values measured by the NPOL3 versus proton kinetic energy T_p values determined by the LAS for the (p,np) reaction of CD_2 (deuterated polyethylene) at $T_0 = 296$ MeV. The color scale (gray scale) is logarithmic.

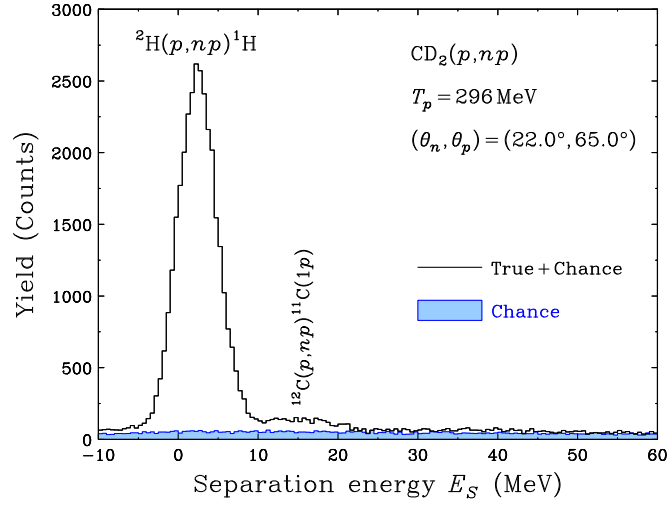

FIG. 3. Separation-energy spectrum for the (p,np) reaction of CD_2 (deuterated polyethylene) at $T_0 = 296$ MeV. The shaded area corresponds to the background from chance coincident events. See text for details.

thickness of the ^{12}C target. The energy resolution was determined by assessing the ^{12}C$(p,n)^{12}$N$(4^-; 4.2$ MeV) reaction, and the resulting value was 4 MeV at FWHM.

B. Neutron and proton coincident measurements

Figure 2 presents the neutron energy T_n and proton energy T_p spectra for the CD$_2(p,np)$ reaction at 296 MeV. In the case of a $A(p,np)B$ reaction with a target nucleus A and a residual nucleus B, the separation energy E_S is given by

$$E_S = T_0 - (T_p + T_n + T_B) = E_x - Q, \qquad (1)$$

where T_B is the kinetic energy of the residual nucleus, E_x is the excitation energy, and Q is the reaction Q value. The separation-energy spectrum up to 60 MeV is shown in Fig. 3. True and chance coincident events were distinguished by the neutron and proton time-of-flight (TOF) difference determined by the NPOL3 and LAS systems, and the contribution from the chance events is indicated in this figure by the shaded histogram. A prominent peak related to the $1s$ knockout ^{2}H(p,np) reaction is observed, with an overall energy resolution of approximately 6 MeV at FWHM. The yield from the $1p$ knockout ^{12}C(p,np) reaction is also evident, at $E_S \simeq 15$ MeV.

IV. THEORETICAL MODELS

The experimental data were compared with the results of theoretical calculations to investigate the nuclear medium effects on the NN interaction. These calculations were performed using the THREEDEE computer code [35]. In order to compare the experimental results with the theoretical predictions, the theoretical calculations were averaged over the angular and momentum acceptances of the NPOL3 and the LAS. Since the formalism for the theoretical calculations has been presented in Refs. [35,36], only a brief description relevant to the present analysis is provided herein.

A. Structure model

The bound-state wave function for ^{2}H was obtained by calculating the Argonne v_{18} high-quality NN potential [37], which reproduces the deuteron properties very well. The single-particle wave functions for ^{6}Li and ^{12}C were generated using Woods-Saxon (WS) potentials. The WS geometrical parameters, r_0 and a, and the depths of the spin-orbit potentials, V_{so}, were taken from the parametrization by Elton and Swift [38]. The depths of the WS potentials have been adjusted to reproduce the empirical separation energies of the bound nucleons.

B. Reaction model

The NN t matrices were parameterized based on the solution to Arndt's phase-shift analysis [39], and the effective two-body kinetic energy and scattering angle were obtained with the so-called final energy prescription [40]. The conventional medium effects were also investigated using the g matrix obtained by solving the Bethe-Goldstone equation [41,42]. The effects of nonlocal potentials were included on an approximate basis by applying the Perey correction factor of $\beta = 0.85$ fm [43]. It should be noted that the absolute values of the cross sections are sensitive to this factor. The calculations for ^{2}H were performed applying the PWIA, whereas those for ^{6}Li and ^{12}C were carried out with the DWIA. The distorted waves for incident and outgoing particles were calculated using global optical potentials based on Dirac phenomenology [44].

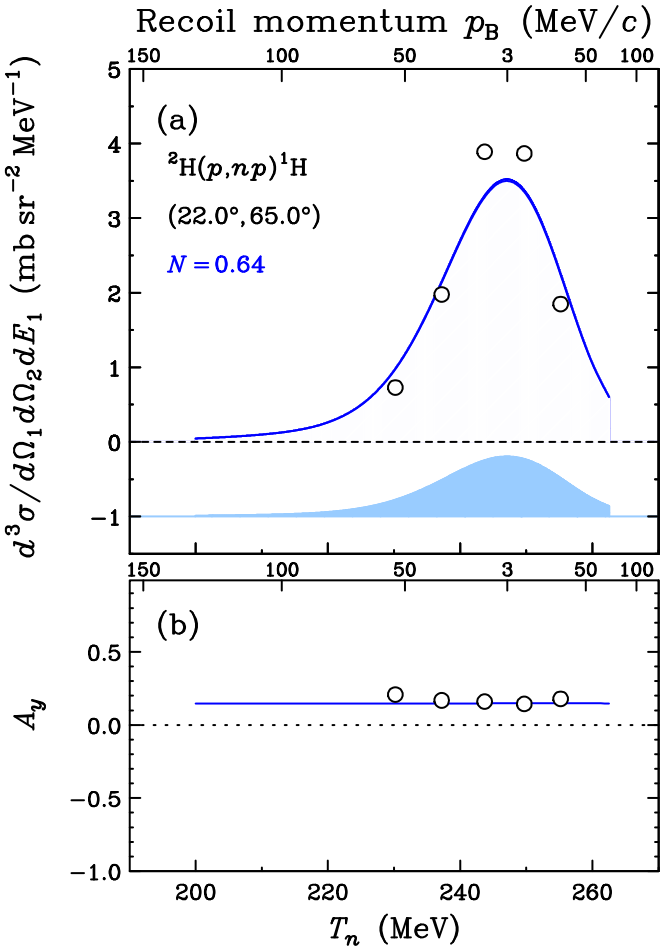

FIG. 4. (a) Cross sections and (b) analyzing powers for the 1s knockout ^{2}H(p,np) reaction at $T_0 = 296$ MeV as functions of both the neutron energy T_n and the recoil momentum p_B. The solid curves represent the results of PWIA calculations. The shaded area represents the fitting uncertainty of the cross sections. See text for detail.

C. Spectroscopic factor

The triple-differential cross section in the laboratory frame can be written as

$$\sigma(E_S,T_n) = \frac{d^3\sigma}{d\Omega_n d\Omega_p dT_n}, \tag{2}$$

where $d\Omega_n$ and $d\Omega_p$ represent the NPOL3 and LAS solid angles, respectively. Herein, the spectroscopic factor S is defined as

$$\sigma^{\rm exp}(E_S,T_n) = S\sigma^{\rm calc}(E_S,T_n), \tag{3}$$

where $\sigma^{\rm exp}(E_S,T_n)$ and $\sigma^{\rm calc}(E_S,T_n)$ are the experimental and theoretical cross sections, respectively. Note that the theoretical cross section $\sigma^{\rm calc}(E_S,T_n)$ is the single-particle cross section for a single target neutron.

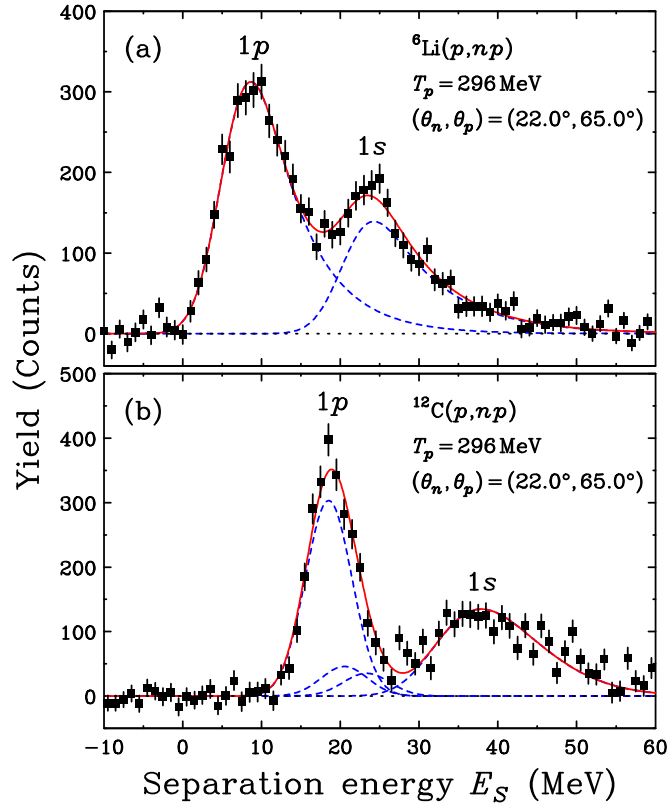

FIG. 5. Separation-energy spectra for (a) ^{6}Li(p,np) and (b) ^{12}C(p,np) reactions at $T_0 = 296$ MeV. The dashed curves represent the fits to the individual peaks and the solid curve shows the sum of the peak fitting.

V. RESULTS AND DISCUSSIONS

A. ^{2}H

Figure 4 shows the cross sections and analyzing powers obtained for the 1s knockout ^{2}H(p,np) reaction as functions of both the neutron energy T_n and the recoil momentum p_B. Note that the recoil momentum p_B corresponds to the proton momentum in the target nucleus at the plane-wave limit. Since the nucleon momentum distribution in a nucleus is related to the orbital angular momentum, L, the recoil-momentum distribution of the cross section will clearly vary with L. The cross-section data exhibit a maximum at $p_B \simeq 0$ MeV/c in the recoil-momentum distribution, which is characteristic for the 1s ($L = 0$) knockout reaction. The solid curves in Fig. 4 show the results of the theoretical calculations, from which it can be seen that the calculations for the analyzing power are in good agreement with the experimental data. In contrast, the theoretical results for the cross section must be normalized by a factor of $N = 0.64 \pm 0.15$. A similar overestimation resulting from PWIA calculations has been reported for the ^{2}H(p,np) reaction at $T_0 = 200$ MeV with $N = 0.4$–0.9 [45]. It should be noted that Witała *et al.* [46] have successfully reproduced these data in the framework of the Faddeev calculations by including relativistic effects. Since the relativistic effects would be significantly greater at higher energies, further detailed theoretical investigations including the present data are required to assess

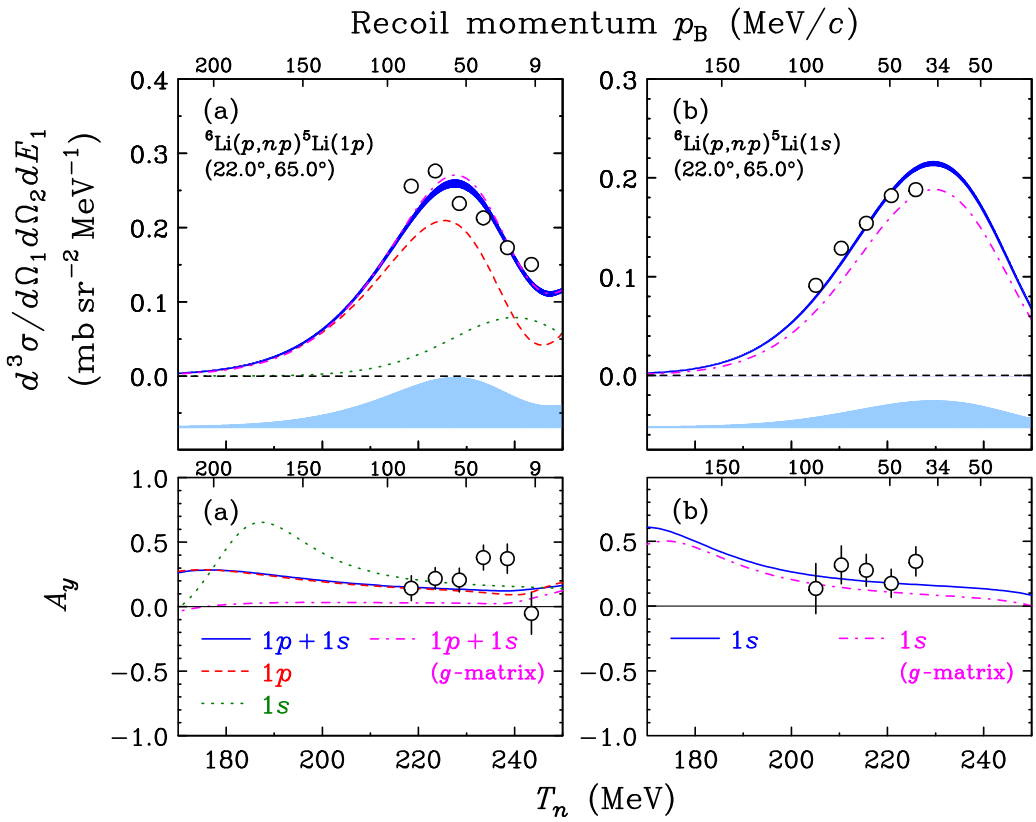

FIG. 6. Cross sections (upper panels) and analyzing powers (lower panels) for (a) $1p$ and (b) $1s$ knockout ^{6}Li(p,np) reactions at $T_0 =$ 296 MeV as functions of both the neutron energy T_n and the recoil momentum p_B. The solid, dashed, and dotted curves show the results of DWIA calculations using the free NN t-matrix, whereas the dot-dashed curves are the DWIA results employing the effective NN g-matrix. The shaded areas represent the fitting uncertainties of the cross sections. See text for detail.

the relativistic effects on the deuteron breakup ^{2}H(p,np) reaction.

B. ^{6}Li and ^{12}C

Figures 5(a) and 5(b) show the separation-energy spectra acquired from the (p,np) reactions of ^{6}Li and ^{12}C, respectively. The contributions from the chance coincident events have been subtracted based on the neutron and proton TOF difference. Here, $1p$ and $1s$ states are clearly observed in both spectra. The dashed curves represent the fits to the individual peaks while the solid curve represents the peak fitting sums. In the case of ^{6}Li, the tail components [47] in both $1p$ and $1s$ states have been taken into account using the asymmetric function Y as in

$$Y(x) = \exp\left(-\frac{x^2}{2\sigma^2}\right) + \left[1 - \exp\left(-\frac{x^2}{2\sigma^2}\right)\right] \cdot H(x) \cdot \exp\left(-k\frac{x}{\sigma}\right), \quad (4)$$

with

$$x = E_S - \bar{E}_S, \quad (5)$$

where H is a Heaviside step function, $\bar{E}_S$ is the peak position, σ is the width parameter, and k is the parameter for the tail component. For ^{12}C, the $1p$ peak was assumed to be the sum of three narrow states at excitation energies of $E_x = 0.0$, 2.0, and 4.8 MeV with $J^\pi = 3/2^-$, $1/2^-$, and $3/2^-$, respectively [48]. The relative strength was fixed equal to that of the corresponding proton S factors [49] assuming isospin symmetry. An asymmetrical Gaussian energy distribution was assumed for the deep-hole $1s$ state [50,51], the FWHM Γ of which depends on E_S as [52]

$$\Gamma(E_S) = \frac{(24\,\text{MeV}) \cdot (E_S - E_F)^2}{(500\,\text{MeV}^2) + (E_S - E_F)^2}, \quad (6)$$

where E_F is the Fermi energy. All peaks were convoluted with a resolution function based on the width of the narrow peaks, and the peak fittings were satisfactory with regard to extracting the $1p$ and $1s$ yields.

Figures 6 and 7 show the cross sections and analyzing powers for $1p$ and $1s$ knockout (p,np) reactions of ^{6}Li and ^{12}C, respectively, as functions of both the neutron energy, T_n, and the recoil momentum, p_B. In both cases, the recoil-momentum distribution of the cross section for the $1s$ knockout reaction has a characteristic feature with a maximum located at approximately the minimum p_B value, whereas the distribution for the $1p$ knockout reaction has a maximum at a finite momentum of $p_B \simeq 70$ MeV/c. It should be noted that the recoil-momentum distributions for both the ^{6}Li and ^{12}C targets are significantly broader than that for the ^{2}H due to their larger Fermi momenta. The solid curves in Figs. 6 and

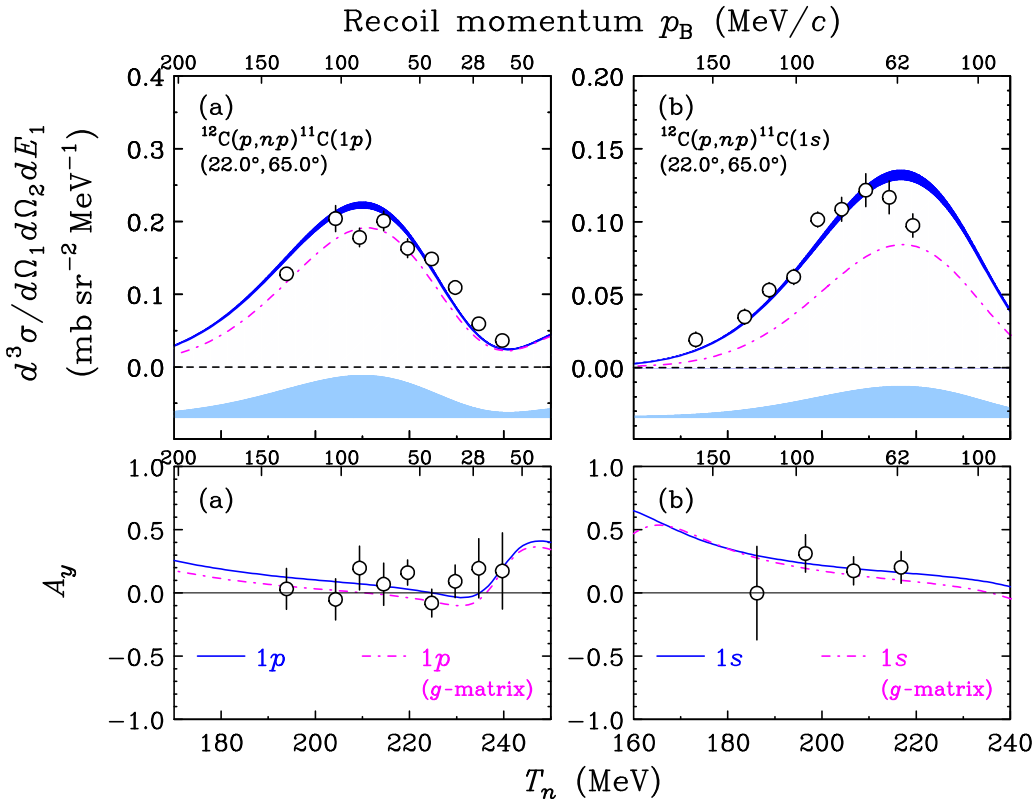

FIG. 7. The same data as in Fig. 6, but for (a) $1p$ and (b) $1s$ knockout ^{12}C(p,np) reactions.

7 present the results of DWIA calculations. In the case of the $1p$ knockout of ^{6}Li, the contribution from the S-wave component has also been taken into consideration since a significant contribution was observed for the relevant proton knockout reaction in ^{6}Li(e,$e'p$) [47]. The contributions from the $1p$ and $1s$ components were determined to reproduce the experimental data, and are indicated by dashed and dotted curves, respectively.

The S factors of the cross sections were determined to reproduce the experimental data when using Eq. (3), and the results are summarized in Table I. The first type of uncertainty in the $S(p,np)$ values corresponds to the statistical uncertainties associated with the data, and is shown by the thicknesses of the curves in Figs. 6 and 7. The second type represents the uncertainties estimated from the fitting quality, and is indicated by the shaded areas. The neutron S factors were found to be significantly larger than the corresponding proton S factors determined from the $(e,e'p)$ data. The reduction of S in the $(e,e'p)$ reaction relative to the independent particle-shell model (IPSM) limit is primarily due to the short-range and long-range correlations [53]. In the range of $P_B = 300$–$600\,\mathrm{MeV}/c$, the tensor interaction primarily generates spin-1 and isospin-0 neutron-proton pairs [54–56] with large relative and small center-of-mass momenta [57–60]. This np-pair dominance causes a greater fraction of protons than neutrons to have high momenta in asymmetric neutron-rich nuclei [61,62], which in turn results in different proton and neutron S factors. However, in the present symmetric nuclei, the neutron S factors are expected to be similar to the corresponding proton S factors. At $T_0 = 200$ MeV, the results were similar for $1p_{3/2}$ and $1p_{1/2}$ knockout (p,np) reactions of ^{12}C [63]. In contrast, at $T_0 = 505$ MeV, the neutron S factors for the $1p_{3/2}$ and $1p_{1/2}$ orbits of ^{16}O were consistent with the corresponding proton S factors [64].

Figure 8 summarizes the S factor ratios between the $(e,e'p)$ and (p,np) values as a function of T_0. The deviation from unity decreased with increases in the incident energy, T_0, and the factor ratio was consistent with unity at $T_0 \simeq 500$ MeV. It should be noted that the proton S factors obtained from the $(p,2p)$ reaction at $T_0 \simeq 200$–500 MeV were consistent with the corresponding $(e,e'p)$ values within approximately 15% [18,65–67]. Part of the observed deviation can be attributed to the ambiguities in the nonlocal corrections and optical potentials in the DWIA calculations, which are estimated to be on the order of 20% in the case of the S factors. However, these effects will depend significantly on the kinematical condition, whereas the present data only relate to a specific condition. Therefore, further theoretical and experimental investigations are required to resolve the discrepancies between the experimentally observed proton and neutron S factors.

In the case of the analyzing powers, the $1s$ data for both ^{6}Li and ^{12}C are consistent with the ^{2}H data. This outcome contradicts previously reported $(p,2p)$ results [17–19,22,69,70], in which a distinct reduction of A_y from the free $\vec{p}+p$ value has been observed for nuclear targets. It is also clear that the conventional medium effects are small and that the results of DWIA calculations shown as the solid and

TABLE I. Spectroscopic factors determined from $(e,e'p)$ and (p,np) reactions.

Target	Orbit	$S(e,e'p)$	Ref.	$S(p,np)$
^{6}Li	$1p$	0.79 ± 0.10	[47]	$1.39 \pm 0.03 \pm 0.30$
	$1s$	0.83 ± 0.08	[68]	$1.67 \pm 0.02 \pm 0.21$
^{12}C	$1p$	2.18 ± 0.11	[49]	$3.94 \pm 0.09 \pm 1.02$
	$1s$			$2.32 \pm 0.07 \pm 0.37$

dot-dashed curves in Figs. 6 and 7 reasonably reproduce the data for both $1s$ and $1p$ knockout reactions.

The reduction of A_y in the case of the $(p,2p)$ reaction has often been discussed in connection with the effective mean density $\bar{\rho}$ [17,71–73]. In general, the $(p,2p)$ and (p,np) reactions primarily occur in the peripheral region of the target nucleus due to the strong absorption effects on both incident and outgoing nucleons. However, the deeply bound $1s$ knockout reaction offers an exceptionally useful means of investigating a high-density region in which $\bar{\rho}$ is greater than 40% of the saturation density. It was found that the A_y reduction increases monotonically as a function of $\bar{\rho}$, suggesting the density dependence of the effective NN interaction in the nuclear field. For comparative purposes, our $1s$ data are presented in Fig. 9 as a function of $\bar{\rho}$. Note that $\bar{\rho}$ for ^{6}Li is significantly smaller than that for ^{12}C due to its $\alpha + d$ [or $\alpha + (p\text{-}n)$ pair] cluster structure. In contrast to the $(p,2p)$ data, the present (p,np) data do not decrease with $\bar{\rho}$. The DWIA and PWIA predictions based on the free NNt matrix are indicated by solid and dashed lines, respectively, and the DWIA results obtained using the effective NN g matrix are also indicated by the dot-dashed line. Both the distortion and conventional medium effects were evidently not significant, and the DWIA calculation employing the free NN t matrix reproduces the present data fairly well. Therefore, we conclude that there is no reduction in the analyzing power of a (p,np) reaction of a nuclear target in the case that the outgoing neutrons are measured at forward angles.

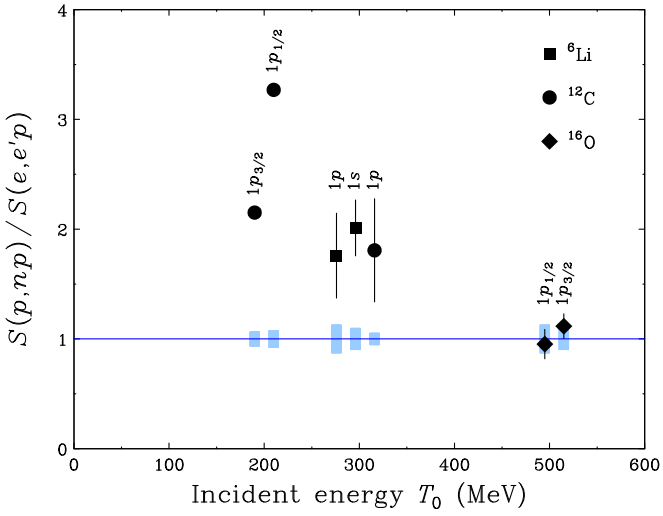

FIG. 8. Ratios of the neutron spectroscopic factors $S(p,np)$ determined from the (p,np) reaction relative to the relevant proton spectroscopic factors $S(e,e'p)$ obtained from the $(e,e'p)$ reaction as a function of incident energy T_0. The shaded boxes represent the uncertainties of $S(e,e'p)$.

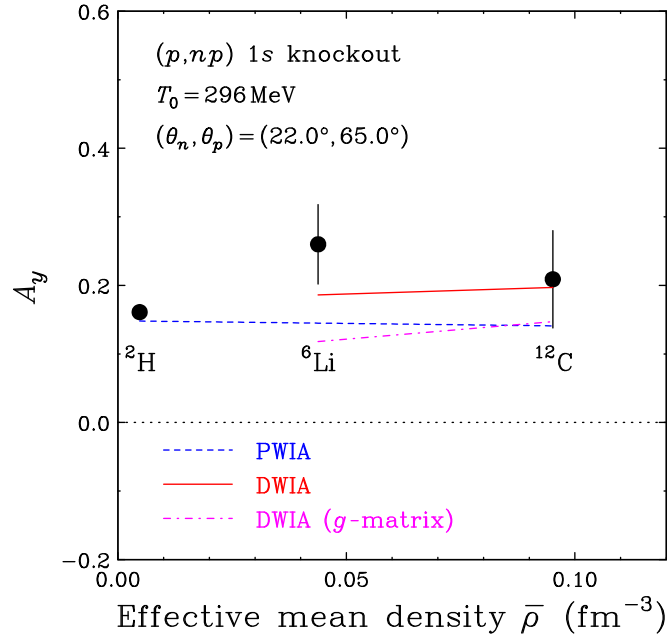

FIG. 9. Analyzing power for the $1s$ knockout (p,np) reactions at $T_0 = 296$ MeV and $(\theta_n,\theta_p) = (22.0°,65.0°)$ as a function of effective mean density $\bar{\rho}$. The solid and dashed lines represent the DWIA and PWIA predictions based on the free NN t-matrix, whereas the dot-dashed line denotes the DWIA prediction based on the effective NN g-matrix.

The remarkable A_y reduction in the case of inclusive (p,p') quasielastic scattering was first predicted by the relativistic model as the result of nucleon mass reduction in a relativistic strong scalar field [74]. A significantly smaller effect was subsequently predicted for the charge-exchange (p,n) reaction [75], which suggests the isospin dependence of the relativistic effect. We have previously investigated the effect of nucleon mass reduction in nuclei using the Horowitz-Love-Franey (HLF) representation of the NN amplitudes [76]. The linear density dependence of the effective nucleon mass M_N^* is given by

$$M_N^* = [1 - C(\bar{\rho}/\rho_0)]M_N, \tag{7}$$

where M_N is the free nucleon mass, $\rho_0 = 0.18\,\mathrm{fm}^{-3}$ [19] is the nuclear saturation density, and $C = 0.18$ [77]. Figure 10(a) compares our data with the HLF calculation employing M_N^*, which corresponds to the PWIA prediction for the (p,np) reaction. A comparison of the $(p,2p)$ data at $T_0 = 392$ MeV and forward proton angle $\theta_1 = 25.5°$ [17] is also shown in Fig. 10(b). Here, the unfilled boxes denote the data for free NN scattering [78], while the dot-dashed and dashed lines correspond to the results obtained with the free mass M_N and effective mass M_N^*, respectively. Note that the $\bar{\rho}$ dependence of the free M_N is due to the finite Q values for nuclear targets. The effective mass correction is very small for (p,np) but

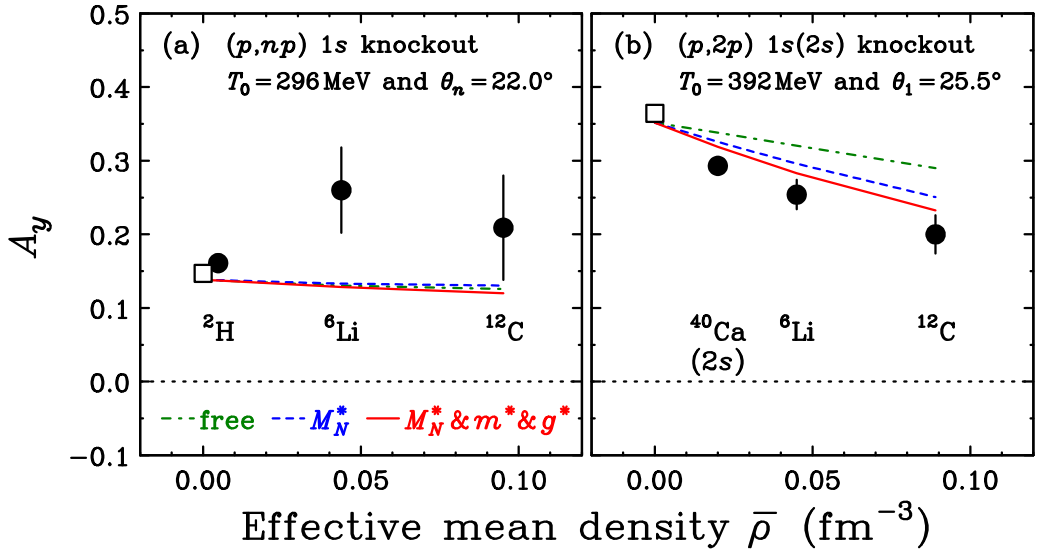

FIG. 10. Comparison of the data for (a) the present (p,np) reaction and (b) the $(p,2p)$ [17] reaction with the PWIA predictions based on the free nucleon mass M_N (dot-dashed) and effective nucleon mass M_N^* (dashed). The solid lines represent the predictions employing both M_N^* and medium modified meson masses m^* and coupling constants g^*. The unfilled boxes denote the data for free NN scattering [78]. See text for detail.

is significant for $(p,2p)$, and reasonably reproduces the $\bar{\rho}$ dependence of both (p,np) and $(p,2p)$ data.

Finally, in order to investigate the nonconventional medium effects in (p,np) and $(p,2p)$ reactions, we employed the Brown-Rho scaling conjecture [13] as applied by Krein *et al.* [79], given by

$$\frac{m^*}{m} = \frac{g^*}{g} = 1 - C\frac{\bar{\rho}}{\rho_0}, \tag{8}$$

where (m,g) and (m^*,g^*) are free and medium-modified meson masses and coupling constants, respectively. Note that the pion mass and coupling constant are not affected due to the Goldstone nature of the pion. The scaling conjecture was implemented based on the relativistic HLF model [76], and the results obtained with $C = 0.18$ [77] are shown in Fig. 10 by the solid lines. The m^* and g^* corrections were relatively small compared with those generated by M_N^*, and better describe the $(p,2p)$ data. It should be noted that the polarization transfer D_{NN} for $(p,2p)$ reactions cannot be explained by calculations based on the Brown-Rho scaling conjecture [80]. Furthermore, the A_y reduction for inclusive (p,p') quasielastic scattering has been explained in the nonrelativistic model by the conventional medium effects of the NN interaction as well as the distortion effects [81]. Therefore, further theoretical investigations are needed in order to assess the isospin and density dependences of the nuclear medium effects on the NN interaction.

VI. SUMMARY AND CONCLUSION

We have presented the cross sections and analyzing powers for (p,np) reactions of ^{2}H, ^{6}Li, and ^{12}C at $T_0 = 296$ MeV. The $1s$ and $1p$ knockout reactions were successfully separated, and recoil-momentum distributions of the associated cross sections clearly varied with the corresponding single-particle orbitals. These data were compared with the results of PWIA and DWIA calculations employing a free NN interaction. The angular distributions of the cross sections were found to be reproduced reasonably well by the calculations, and the S-wave component appears to make a sizable contribution to the $1p$ knockout of ^{6}Li. In contrast, the neutron S factors were significantly larger than the corresponding proton S factors determined from the $(e,e'p)$ data. Part of this difference could be due to the ambiguities in the nonlocal corrections and optical potentials in the present DWIA calculations, although further theoretical and experimental investigations are required to resolve the discrepancy.

The results of DWIA and PWIA calculations agree reasonably well with experimental values for analyzing powers, in contrast to the $(p,2p)$ data, which are significantly reduced relative to the calculation values. Part of the difference in the medium effects between the (p,np) and $(p,2p)$ reactions can be explained by the relativistic effect of nucleon mass reduction in the nuclear field. The present findings, in conjunction with further experimental studies based on polarization transfer measurements, should provide valuable insights into the nuclear medium effects on the NN interaction.

ACKNOWLEDGMENTS

The authors are grateful to Professor K. Ogata and Dr. K. Minomo for valuable discussions. We also acknowledge the outstanding work of the RCNP accelerator group with regard to ensuring a high-quality polarized proton beam. The experimental work was performed at RCNP under Program No. E367. This research was also supported in part by the Ministry of Education, Culture, Sports, Science, and Technology of Japan.

[1] J. M. Moss, Phys. Rev. C **26**, 727 (1982).
[2] E. Bleszynski, M. Bleszynski, and C. A. Whitten, Phys. Rev. C **26**, 2063 (1982).
[3] R. Brockmann and R. Machleidt, Phys. Rev. C **42**, 1965 (1990).
[4] H. Müther, R. Machleidt, and R. Brockmann, Phys. Rev. C **42**, 1981 (1990).
[5] F. Sammarruca and P. Krastev, Phys. Rev. C **73**, 014001 (2006).
[6] F. Sammarruca, Phys. Rev. C **77**, 047301 (2008).
[7] F. Sammarruca, B. Chen, L. Coraggio, N. Itaco, and R. Machleidt, Phys. Rev. C **86**, 054317 (2012).
[8] M. Ichimura, H. Sakai, and T. Wakasa, Prog. Part. Nucl. Phys. **56**, 446 (2006).
[9] S. W. Wissink, in *Spin and Isospin in Nuclear Interactions*, edited by S. W. Wissink, C. D. Goodman, and G. E. Walker (Plenum, New York, 1991), p. 253.
[10] E. J. Stephenson and J. A. Tostevin, in *Spin and Isospin in Nuclear Interactions*, edited by S. W. Wissink, C. D. Goodman, and G. E. Walker (Plenum, New York, 1991), p. 281.
[11] H. Baghaei, R. A. Lindgren, P. Slocum, E. J. Stephenson, A. D. Bacher, S. Chang, J. Lisantti, J. Liu, C. Olmer, S. Wells *et al.*, Phys. Rev. Lett. **69**, 2054 (1992).
[12] E. J. Stephenson, J. Liu, A. D. Bacher, S. M. Bowyer, S. Chang, C. Olmer, S. P. Wells, S. W. Wissink, and J. Lisantti, Phys. Rev. Lett. **78**, 1636 (1997).
[13] G. E. Brown and M. Rho, Phys. Rev. Lett. **66**, 2720 (1991).
[14] R. J. Furnstahl, D. K. Griegel, and T. D. Cohen, Phys. Rev. C **46**, 1507 (1992).
[15] T. Hatsuda, Nucl. Phys. A **544**, 27c (1992).
[16] F. Sammarruca, E. J. Stephenson, K. Jiang, J. Liu, C. Olmer, A. K. Opper, and S. W. Wissink, Phys. Rev. C **61**, 014309 (1999).
[17] K. Hatanaka, M. Kawabata, N. Matsuoka, Y. Mizuno, S. Morinobu, M. Nakamura, T. Noro, A. Okihana, K. Sagara, K. Takahisa *et al.*, Phys. Rev. Lett. **78**, 1014 (1997).
[18] C. A. Miller, K. H. Hicks, R. Abegg, M. Ahmad, N. S. Chant, D. Frekers, P. W. Green, L. G. Greeniaus, D. A. Hutcheon, P. Kitching *et al.*, Phys. Rev. C **57**, 1756 (1998).
[19] T. Noro, T. Yonemura, S. Asaji, N. S. Chant, K. Fujita, Y. Hagihara, K. Hatanaka, G. C. Hillhouse, T. Ishida, M. Itoh *et al.*, Phys. Rev. C **72**, 041602 (2005).
[20] T. Noro, T. Baba, K. Hatanaka, M. Ito, M. Kawabata, N. Matsuoka, Y. Mizuno, S. Morinobu, M. Nakamura, A. Okihana *et al.*, Nucl. Phys. A **629**, 324c (1998).
[21] T. Noro, H. Akimune, H. Akiyoshi, I. Daito, H. Fujimura, K. Hatanaka, F. Ihara, T. Ishikawa, M. Ito, M. Kawabata *et al.*, Nucl. Phys. A **663&664**, 517c (2000).
[22] D. S. Carman, L. C. Bland, N. S. Chant, T. Gu, G. M. Huber, J. Huffman, A. Klyachko, B. C. Markham, P. G. Roos, P. Schwandt, and K. Solberg, Phys. Rev. C **59**, 1869 (1999).
[23] T. Noro, Y. Yamada, M. Dozono, Y. Eguchi, N. Fujita, K. Hatanaka, T. Imamura, D. Ishikawa, M. Itoh, S. Kuroita *et al.*, RCNP Annual Report (2009), p. 9.
[24] Y. Yamada, Ph.D. thesis, Kyushu University, 2010.
[25] A. A. Cowley, G. J. Arendse, R. F. Visser, G. F. Steyn, S. V. Förtsch, J. J. Lawrie, J. V. Pilcher, T. Noro, T. Baba, K. Hatanaka *et al.*, Phys. Rev. C **57**, 3185 (1998).
[26] T. Wakasa, K. Hatanaka, Y. Fujita, G. P. A. Berg, H. Fujimura, H. Fujita, M. Itoh, J. Kamiya, T. Kawabata, K. Nagayama *et al.*, Nucl. Instrum. Methods Phys. Res., Sect. A **482**, 79 (2002).
[27] K. Hatanaka, K. Takahisa, H. Tamura, M. Sato, and I. Miura, Nucl. Instrum. Methods Phys. Res., Sect. A **384**, 575 (1997).
[28] M. Kondo, I. Miura, T. Yamazaki, H. Ejiri, A. Shimizu, M. Inoue, K. Hosono, T. Saito, Y. Nagai, H. Sakai *et al.*, in *Proceedings of the 7th International Conference on Cyclotrons and Their Applications, Zurich, Switzerland, 1975*, edited by W. Joho (Birkhäuser, Basel, 1975), p. 95.
[29] I. Miura, T. Yamazaki, A. Shimizu, K. Hosono, T. Itahashi, T. Saito, A. Ando, K. Tamura, K. Hatanaka, M. Kibayashi *et al.*, in *Proceedings of the 13th International Conference on Cyclotrons and Their Applications, Vancouver, Canada, 1992*, edited by G. Dutto and M. K. Craddock (World Scientific, Singapore, 1993), p. 3.
[30] T. Wakasa, H. Sakai, H. Okamura, H. Otsu, S. Fujita, S. Ishida, N. Sakamoto, T. Uesaka, Y. Satou, T. Nonaka *et al.*, Nucl. Instrum. Methods Phys. Res. A **404**, 355 (1998).
[31] http://www.hitachi-m-admet.com/.
[32] T. Wakasa, Y. Hagihara, M. Sasano, S. Asaji, K. Fujita, K. Hatanaka, T. Ishida, T. Kawabata, H. Kuboki, Y. Maeda *et al.*, Nucl. Instrum. Methods Phys. Res., Sect. A **547**, 569 (2005).
[33] N. Matsuoka, T. Noro, K. Sagara, S. Morinobu, A. Okihana, and K. Hatanaka, RCNP Annual Report (1991), p. 186.
[34] M. Dozono, T. Wakasa, E. Ihara, S. Asaji, K. Fujita, K. Hatanaka, M. Ichimura, T. Ishida, T. Kaneda, H. Matsubara *et al.*, Phys. Rev. C **80**, 024319 (2009).
[35] N. S. Chant and P. G. Roos, Phys. Rev. C **27**, 1060 (1983).
[36] G. C. Hillhouse and T. Noro, Phys. Rev. C **74**, 064608 (2006).
[37] R. B. Wiringa, V. G. J. Stoks, and R. Schiavilla, Phys. Rev. C **51**, 38 (1995).
[38] L. R. B. Elton and A. Swift, Nucl. Phys. A **94**, 52 (1967).
[39] R. A. Arndt, C. H. Oh, I. I. Strakovsky, R. L. Workman, and F. Dohrmann, Phys. Rev. C **56**, 3005 (1997).
[40] E. F. Redish, G. J. Stephenson, and G. M. Lerner, Phys. Rev. C **2**, 1665 (1970).
[41] P. J. Dortmans and K. Amos, J. Phys. G **17**, 901 (1991).
[42] P. J. Dortmans and K. Amos, Phys. Rev. C **49**, 1309 (1994).
[43] F. Perey and B. Buck, Nucl. Phys. **32**, 353 (1962).
[44] E. D. Cooper, S. Hama, and B. C. Clark, Phys. Rev. C **80**, 034605 (2009).
[45] W. Pairsuwan, J. W. Watson, M. Ahmad, N. S. Chant, B. S. Flanders, R. Madey, P. J. Pella, and P. G. Roos, Phys. Rev. C **52**, 2552 (1995).
[46] H. Witała, J. Golak, and R. Skibiński, Phys. Lett. B **634**, 374 (2006).
[47] J. B. J. M. Lanen, A. M. van den Berg, H. P. Blok, J. F. J. van den Brand, C. T. Christou, R. Ent, A. G. M. van Hees, E. Jans, G. J. Kramer, L. Lapikás *et al.*, Phys. Rev. Lett. **62**, 2925 (1989).
[48] J. H. Kelley, E. Kwan, J. E. Purcell, C. G. Sheu, and H. R. Weller, Nucl. Phys. A **880**, 88 (2012).
[49] G. van der Steenhoven, H. P. Blok, E. Jans, M. de Jong, L. Lapikás, E. N. M. Quint, and P. K. A. de Witt Huberts, Nucl. Phys. A **480**, 547 (1988).
[50] E. N. M. Quint, Ph.D. thesis, University of Amsterdam, 1988.
[51] J. W. A. den Herder, H. P. Blok, E. Jans, P. H. M. Keizer, L. Lapikás, E. N. M. Quint, G. van der Steenhoven, and P. K. A. de Witt Huberts, Nucl. Phys. A **490**, 507 (1988).
[52] G. E. Brown and M. Rho, Nucl. Phys. A **372**, 397 (1981).
[53] W. H. Dickhoff and C. Barbeieri, Prog. Part. Nucl. Phys. **52**, 377 (2004).
[54] R. Schiavilla, R. B. Wiringa, S. C. Pieper, and J. Carlson, Phys. Rev. Lett. **98**, 132501 (2007).

[55] R. B. Wiringa, R. Schiavilla, S. C. Pieper, and J. Carlson, Phys. Rev. C **78**, 021001 (2008).
[56] R. B. Wiringa, R. Schiavilla, S. C. Pieper, and J. Carlson, Phys. Rev. C **89**, 024305 (2014).
[57] L. L. Frankfurt and M. I. Strikman, Phys. Rep. **76**, 215 (1981).
[58] L. Frankfurt and M. Strikman, Phys. Rep. **160**, 235 (1988).
[59] O. Hen, L. B. Weinstein, E. Piasetzky, G. A. Miller, M. M. Sargsian, and Y. Sagi, Phys. Rev. C **92**, 045205 (2015).
[60] O. Hen, G. A. Miller, E. Piasetzky, and L. B. Weinstein, arXiv:1611.09748 [Rev. Mod. Phys. (to be published)].
[61] T. Frick, H. Müther, A. Rios, A. Polls, and A. Ramos, Phys. Rev. C **71**, 014313 (2005).
[62] O. Hen, M. Sargsian, L. B. Weinstein, E. Piasetzky, H. Hakobyan, D. W. Higinbotham, M. Braverman, W. K. Brooks, S. Gilad, K. P. Adhikari *et al.*, Science **346**, 614 (2014).
[63] D. S. Carman, L. C. Bland, N. S. Chant, T. Gu, G. M. Huber, J. Huffman, A. Klyachko, B. C. Markham, P. G. Roos, P. Schwandt, and K. Solberg, Phys. Lett. B **452**, 8 (1999).
[64] W. J. McDonald, R. N. MacDonald, W. C. Olsen, R. Dymarz, F. Khanna, L. Antonuk, J. M. Cameron, P. Kitching, G. C. Neilson, D. M. Sheppard *et al.*, Nucl. Phys. A **456**, 577 (1986).
[65] T. Noro, H. Sakaguchi, O. V. Miklukho, S. L. Belostotski, K. Hatanaka, J. Kamiya, A. U. Kisselef, H. Takeda, T. Wakasa, Y. Yasuda, and H. P. Yoshida, in *Proceedings of the Kyudai-RCNP International Symposium on Nuclear Many-Body and Medium Effects in Nuclear Interactions and Reactions, Fukuoka, 2002*, edited by K. Hatanaka, T. Noro, K. Sagara, H. Sakaguchi, and H. Sakai (World Scientific, Singapore, 2003), p. 223.
[66] H. Yoshida, Ph.D. thesis, Kyushu University, 2010.
[67] T. Noro, Y. Shindo, M. Tabata, T. Akieda, D. Eto, H. Fujioka, G. Guillaume, K. Hatanaka, C. Iwamoto, H. Kon *et al.*, RCNP Annual Report (2015).
[68] J. B. J. M. Lanen, R. G. Lovas, A. T. Kruppa, H. P. Blok, J. F. J. van den Brand, R. Ent, E. Jans, G. J. Kramer, L. Lapikás, E. N. M. Quint *et al.*, Phys. Rev. Lett. **63**, 2793 (1989).
[69] C. A. Miller, R. Abegg, D. Frekers, P. W. Green, K. Hicks, D. A. Hutcheon, M. Ahmad, L. G. Greeniaus, P. Kitching, D. Mack *et al.*, J. Phys. Colloques **51**, C6 (1990).
[70] V. A. Andreev, M. N. Andronenko, G. M. Amalsky, S. L. Belostotski, O. A. Domchenkov, O. Y. Fedorov, K. Hatanaka, A. A. Izotov, A. A. Jgoun, J. Kamiya *et al.*, Phys. Rev. C **69**, 024604 (2004).
[71] B. Van Overmeire, W. Cosyn, P. Lava, and J. Ryckebusch, Phys. Rev. C **73**, 064603 (2006).
[72] W. Cosyn and J. Ryckebusch, Phys. Rev. C **80**, 011602 (2009).
[73] J. Ryckebusch, W. Cosyn, and M. Vanhalst, Phys. Rev. C **83**, 054601 (2011).
[74] C. J. Horowitz and M. J. Iqbal, Phys. Rev. C **33**, 2059 (1986).
[75] G. C. Hillhouse, B. I. S. van der Ventel, S. M. Wyngaardt, and P. R. De Kock, Phys. Rev. C **57**, 448 (1998).
[76] C. J. Horowitz, Phys. Rev. C **31**, 1340 (1985).
[77] T. Hatsuda and S. H. Lee, Phys. Rev. C **46**, R34 (1992).
[78] R. L. Workman, W. J. Briscoe, and I. I. Strakovsky, Phys. Rev. C **94**, 065203 (2016).
[79] G. Krein, T. A. J. Maris, B. B. Rodrigues, and E. A. Veit, Phys. Rev. C **51**, 2646 (1995).
[80] T. Noro, M. Kawabata, G. C. Hillhouse, S. Akimune, H. Akiyoshi, I. Daito, K. Hatanaka, M. Itoh, Y. Maeda, N. Matsuoka *et al.*, Phys. Rev. C **77**, 044604 (2008).
[81] K. Ogata, G. C. Hillhouse, and B. I. S. van der Ventel, Phys. Rev. C **76**, 021602 (2007).